Catalysis Today 142 (2009) 114–124

Contents lists available at ScienceDirect

Catalysis Today

journal homepage: www.elsevier.com/locate/cattod

The design of Ti-, V-, Cr-oxide single-site catalysts within zeolite frameworks and their photocatalytic reactivity for the decomposition of undesirable molecules—The role of their excited states and reaction mechanisms

Masakazu Anpo *, Tae-Ho Kim, Masaya Matsuoka

Department of Applied Chemistry, Graduate School of Engineering, Osaka Prefecture University, 1-1 Gakuen-cho, Naka-ku, Sakai, Osaka 599-8531, Japan

ARTICLE INFO

Article history:
Available online 9 January 2009

Keywords:
Single-site catalyst
Photocatalysis
Transition metal oxide species
Charge-transfer excited state
Electron–hole pair state
Zeolites
Mesoporous molecular sieves
NOx decomposition
CO_2 reduction
Preferential oxidation of CO in H_2 (PROX)

ABSTRACT

Transition metal oxides (Ti, V, Mo, Cr, etc.) incorporated within the framework of zeolites were found to exhibit high and unique photocatalytic reactivity as single-site heterogeneous catalysts for various reactions such as the decomposition of NOx (NO, N_2O) into N_2 and O_2, the reduction of CO_2 with H_2O to produce CH_4 and CH_3OH, the preferential oxidation of CO in the presence of H_2 (PROX), the partial oxidation of various hydrocarbons with O_2 or NO or N_2O and the epoxidation and metathesis reaction of alkenes. In situ spectroscopic investigations of these photofunctional systems applying photoluminescence, XAFS (XANES and FT-EXAFS), ESR and FT-IR revealed that the photo-excited states of the transition metal oxides play a vital role in the photocatalytic reactions. The high photocatalytic efficiency and selectivity of these single-site catalysts for significant reactions, which could not be observed with semiconducting bulk photocatalysts, were found to depend strongly on the unique and isolated local structure of the catalysts constructed within the restricted framework structure of the zeolites.

1. Introduction

One of the most important challenges facing scientists today is how to utilize clean and abundant solar energy and convert it into useful chemical energy, especially for applications in environmentally friendly catalysts that can reduce toxic pollutants in the atmosphere and water as well as for the production of clean energy resources. To address such concerns, the development of various types of semiconducting bulk photocatalysts have been intensively carried out with such successful results as the elimination of NOx in air [1,2], the degradation of toxic organic pollutants diluted in water [3,4], and the decomposition of water into H_2 and O_2 with a separate evolution [5,6]. In addition to these semiconducting bulk photocatalysts, the unique photocatalytic properties of single-site catalysts constructed on various support surfaces such as SiO_2 as well as within zeolites frameworks or cavities by impregnation, grafting or anchoring methods and the hydrothermal synthesis of transition metal oxide-incorporated zeolites also have the potential for many new applications in photofunctional systems [7–32].

As shown in Eq. (1), highly dispersed and isolated transition metal oxides, such as Ti, V, Mo, and Fe can be excited under UV or visible light (or sunlight) irradiation for Cr-oxides to form corresponding charge-transfer excited states involving an electron transfer from $O^{2-}{}_{(l)}$ to $M^{n+}{}_{(l)}$:

$$[M^{n+} - O^{2-}]_{(l)} \xrightarrow{h\nu} [M^{(n-1)+} - O^{-}]^{*}_{(l)} \quad (M: \text{Ti, V, Cr, Mo,...}) \tag{1}$$

The high reactivity and selectivity of these charge-transfer excited states formed on single-site heterogeneous catalysts, in which the electron–hole pair states are localized in close proximity, led to such significant photocatalytic reactions as the decomposition of NOx (NO and N_2O) into N_2 and O_2 [9–16,20], the partial oxidation of hydrocarbons with O_2 or NO [9–16,24,25], the degradation of organic pollutants dissolved in water [33–35], and the reduction of CO_2 with H_2O to produce CH_4 and CH_3OH [9–19]. This is in stark contrast to semiconducting bulk photocatalysts in which the photo-formed electrons and holes have large distant spaces between them (charge separation), thus, leading to different reaction mechanisms. These findings indicate that a fundamental understanding of the coordination structure and electronic state of the active surface species, as well as the bulk crystalline structure and electronic properties, is important in the design of applicable photocatalytic systems having high reactivity and selectivity.

* Corresponding author. Fax: +81 72 254 9910.
E-mail address: anpo@chem.osakafu-u.ac.jp (M. Anpo).

0920-5861/$ – see front matter © 2008 Elsevier B.V. All rights reserved.
doi:10.1016/j.cattod.2008.11.006

In the present paper, the photocatalytic reactivities of various single-site transition metal oxide photocatalyst species such as Ti, V, Mo and Cr have been summarized. The local structures of these single-site oxides are discussed based on the results obtained by various in situ spectroscopic techniques. Special attention has been focused on the relationship between the local structures of the single-site catalysts and their photocatalytic reactivity and selectivity for various photocatalytic reactions.

2. Photocatalytic reactivity of Ti-oxide species constructed within zeolite cavities

In the use of solar energy through chemical storage, the design of highly efficient and selective photocatalytic systems that work without any loss is of vital interest. In particular, the development of efficient photocatalytic systems that are able to decompose NO directly into N_2 and O_2 or to reduce CO_2 with H_2O into chemically valuable compounds such as CH_4 or CH_3OH is one of the most desired and challenging goals in the research of environmentally friendly catalysts [9–16]. We have reported that these photocatalytic reactions were successfully able to proceed on powdered TiO_2 at room temperature [36,37]. Using various types of well-characterized powdered TiO_2 catalysts, the effect of the structure on the catalytic activity was investigated. Extremely small TiO_2 particles having large band gaps were found to show the highest reactivity [36]. At the same time, the activity of the highly dispersed Ti-oxide species anchored onto silica glass or zeolite was also investigated [9–19] and it was found that a highly dispersed Ti-oxide species exhibits unique, high photocatalytic reactivity as compared to bulk TiO_2 powder, i.e., the formation of N_2 and O_2 in the decomposition of NO as well as the formation of CH_3OH in the reduction of CO_2 with H_2O were observed and the product selectivity increased as the extent of the dispersion of the Ti-oxide species became higher [9–19]. These results indicate that by using zeolites as supports, highly dispersed Ti-oxides species can be produced, leading to the development of environmentally friendly photocatalytic systems having high catalytic efficiency, selectivity and other fascinating properties such as shape selectivity and a reactant gas condensation effect, which can be derived from the physicochemical properties of zeolites.

2.1. Photocatalytic reduction of CO_2 with H_2O on Ti-oxide single-site catalysts constructed within zeolite cavities

A Ti-oxide/Y-zeolite (1.1 wt.% as TiO_2) was prepared by ion-exchange with an aqueous titanium ammonium oxalate solution using Y-zeolite sample (SiO_2/Al_2O_3 = 5.5) (ex-Ti-oxide/Y-zeolite). The Pt-loaded ex-Ti-oxide/Y-zeolite (1.0 wt.% as Pt) was prepared by impregnation with an aqueous solution of H_2PtCl_6. UV-irradiation of powdered TiO_2 and Ti-oxide/Y-zeolite catalysts prepared by ion-exchange or impregnation methods in the presence of a mixture of CO_2 and H_2O led to the evolution of CH_4 and CH_3OH in the gas phase at 328 K, as well as trace amounts of CO, C_2H_4 and C_2H_6. The evolution of small amount of O_2 was also observed. As shown in Fig. 1, the yields of these photo-formed products increase linearly as a function of the UV-irradiation time and the reaction immediately ceases when irradiation is discontinued, indicating the photocatalytic reduction of CO_2 with H_2O on the catalysts. The specific photocatalytic reactivities for the formation of CH_4 and CH_3OH are shown in Fig. 2. It is clear that the photocatalytic reaction rate and selectivity for the formation of CH_3OH depend strongly on the type of catalyst. It can be seen that the specific photocatalytic reactivities of the Ti-oxide/Y-zeolite catalysts, which have been normalized by unit gram of Ti in the catalysts, are much higher than bulk TiO_2. The ex-Ti-oxide/Y-zeolite exhibits a high reactivity and a high selectivity for the formation of CH_3OH, while the formation of CH_4 was found to be the major reaction on bulk TiO_2 as well as on the imp-Ti-oxide/Y-zeolite.

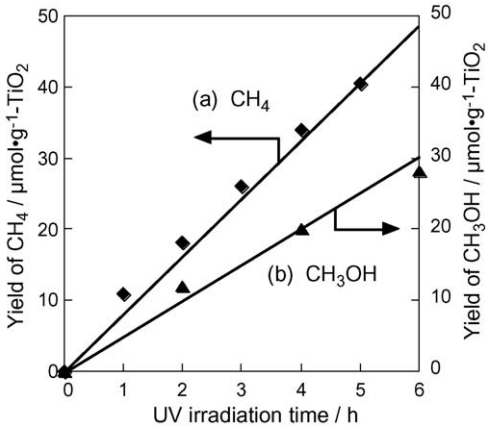

Fig. 1. The reaction–time profiles of the photocatalytic reduction of CO_2 with H_2O to produce CH_4 (a) and CH_3OH (b) on the ex-Ti-oxide/Y-zeolite catalysts.

The ex-Ti-oxide/Y-zeolite exhibited an intense single pre-edge peak, indicating that the Ti-oxide species exists in tetrahedral coordination [17,20]. On the other hand, the imp-Ti-oxide/Y-zeolite exhibited three characteristic weak pre-edge peaks attributed to crystalline anatase TiO_2. Curve-fitting analysis of the EXAFS spectra showed that the ex-Ti-oxide/Y-zeolite catalyst consists of 4-coordinate titanium ions with a coordination number (N) of 3.7 and an atomic distance (R) of 1.78 Å. On the other hand, the imp-Ti-oxide/Y-zeolite catalysts exhibited an intense peak at around 2.7 Å assigned to the neighboring titanium atoms (Ti–O–Ti), indicating the aggregation of the Ti-oxide species in these catalysts.

The ex-Ti-oxide/Y-zeolite catalyst exhibited a photoluminescence spectrum at around 490 nm by excitation at around 290 nm at 77 K. The observed photoluminescence and absorption bands are in good agreement with those previously observed with highly dispersed tetrahedrally coordinated Ti-oxides species prepared in silica matrices [17–20]. It could, therefore, be concluded that the photoluminescence spectrum is attributed to the radiative decay process from the charge-transfer excited state to the ground state of the highly dispersed Ti-oxide species in tetrahedral coordination, as shown below:

$$(Ti^{4+}-O^{2-}) \underset{h\nu'}{\overset{h\nu}{\rightleftarrows}} (Ti^{3+}-O^{-})^{*}$$

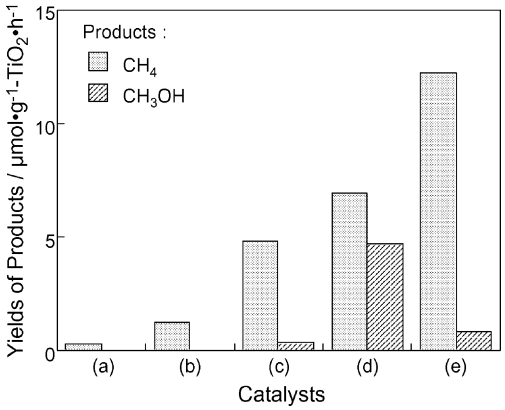

Fig. 2. The product distribution of the photocatalytic reduction of CO_2 with H_2O on anatase TiO_2 powder (a), the imp-Ti-oxide/Y-zeolite (10 wt.% as TiO_2) (b), the imp-Ti-oxide/Y-zeolite (1.0 wt.% as TiO_2) (c), the ex-Ti-oxide/Y-zeolite (1.1 wt.% as TiO_2) (d) and the Pt-loaded ex-Ti-oxide/Y-zeolite (e) catalysts.

On the other hand, the imp-Ti-oxide/Y-zeolite catalysts did not exhibit any photoluminescence. These results, thus, clearly indicate that the ex-Ti-oxide/Y-zeolite catalyst consists of highly dispersed isolated tetrahedral Ti-oxide species while the imp-Ti-oxide/Y-zeolite catalysts involve the aggregated octahedral Ti-oxide species which do not exhibit any photoluminescence spectrum.

The addition of H_2O or CO_2 molecules to the ex-Ti-oxide/Y-zeolite catalyst led to an efficient quenching of the photoluminescence. The lifetime of the charge-transfer excited state was also found to be shortened by the addition of CO_2 or H_2O, its extent depending on the amount of added gasses. Such an efficient quenching of the photoluminescence with CO_2 or H_2O suggests not only that the tetrahedrally coordinated Ti-oxide species is located at positions accessible to the added CO_2 or H_2O but also that the added CO_2 or H_2O interacts and/or reacts with the Ti-oxide species in both its ground and excited states. UV-irradiation of the anchored Ti-oxide catalyst in the presence of CO_2 and H_2O at 77 K led to the appearance of ESR signals due to the Ti^{3+} ions, H atoms, and carbon radicals [17,37]. From these results, the reaction mechanism in the photocatalytic reduction of CO_2 with H_2O on the highly dispersed Ti-oxide catalyst can be proposed, as follows: CO_2 and H_2O molecules interact with the excited state of the photoinduced $(Ti^{3+}–O^-)^*$ species and the reduction of CO_2 and the decomposition of H_2O proceed competitively. Furthermore, H atoms and $OH^•$ radicals are formed from H_2O and react with the carbon species formed from CO_2 to produce CH_4 and CH_3OH.

The addition of CO_2 or H_2O to these zeolites resulted in a significant quenching of the photoluminescence, indicating the excellent accessibility of the Ti-oxide species to CO_2 and H_2O. In addition, quenching with H_2O was observed to be much more effective than with CO_2, reflecting the stronger interaction of H_2O with the Ti-oxide species [17–20]. UV-irradiation of the Ti-mesoporous zeolites and the TS-1 zeolite in the presence of CO_2 and H_2O also led to the formation of CH_3OH and CH_4 as the main products. It was found that Ti-MCM-48 exhibited much higher reactivity than either TS-1 or Ti-MCM-41. Besides the higher dispersion state of the Ti-oxide species, the other distinguishing features of these zeolite catalysts are: TS-1 has a smaller pore size (ca. 5.7 Å) and a three-dimensional channel structure; Ti-MCM-41 has a large pore size (>20 Å) but one-dimensional channel structure; and Ti-MCM-48 has both a large pore size (>20 Å) and three-dimensional channels. The higher reactivity and selectivity for the formation of CH_3OH observed with the Ti-MCM-48 zeolite than with the other catalysts may, thus, be due to the combined contribution of the high dispersion state of the Ti-oxide species and the large pore size with a three-dimensional channel structure. These results strongly indicate that mesoporous zeolites with highly dispersed Ti-oxide species in their framework are promising candidates to act as effective photocatalysts for the reduction of CO_2 with H_2O [15–20].

The effect of Pt-loading on the photocatalytic reactivity of Ti-containing zeolite has also been investigated. Although the addition of Pt onto Ti-containing zeolites was seen to be effective in increasing the photocatalytic reactivity, only the formation of CH_4 is promoted, accompanied by a decrease in the CH_3OH yields. The absorption spectra of the Pt-loaded catalysts were the same as those observed with the original Ti-containing zeolite without Pt-loading. The Pt-loaded catalyst also exhibited the same pre-edge peak in the XANES spectra and the same Ti–O bonding peak in the FT-EXAFS spectra as those of the original Ti-containing zeolite. Moreover, Pt-loading on the Ti-containing zeolite catalyst led to an efficient quenching of the photoluminescence accompanied by a shortening of its lifetime. Since the results of XAFS and absorption measurements indicated that the local structure of the Ti-oxide species dispersed in the zeolite was not altered by Pt loading, the effective quenching of the photoluminescence can be attributed to the electron transfer from the photo-excited Ti-oxide species to metallic Pt existing in the neighborhood of the Ti-oxide species. The electrons are easily transferred from the charge-transfer excited state of the Ti-oxide species, the electron–hole pair state of $(Ti^{3+}–O^-)^*$, to the Pt moieties while the holes remain in the Ti-oxide species, resulting in the charge separation of electrons and holes from the photo-formed electron–hole pair states. As result, on the Pt-loaded Ti-containing zeolite catalyst, photocatalytic reactions that proceed in the same manner as on bulk TiO_2 catalysts became predominant and the reduction reaction by electrons and the oxidation reaction by holes occurred separately on different sites, leading to the selective formation of CH_4.

2.2. Photocatalytic decomposition of NO into N_2 and O_2 on the Ti-oxide single-site catalyst constructed within Y-zeolite cavities

The Ti-oxide/Y-zeolite (1.1 wt.% as TiO_2) was prepared by ion-exchange with an aqueous titanium ammonium oxalate solution using Y-zeolite samples (SiO_2/Al_2O_3 = 5.5) (ex-Ti-oxide/Y-zeolite). Ti-oxide/Y-zeolites having different Ti contents (1.0 and 10 wt.% as TiO_2) were prepared by impregnating the Y-zeolite with an aqueous solution of titanium ammonium oxalate (imp-Ti-oxide/Y-zeolite).

UV-irradiation of the powdered TiO_2 and the Ti-oxide/Y-zeolite catalysts prepared by ion-exchange or impregnation methods in the presence of NO were found to lead to the evolution of N_2, O_2 and N_2O in the gas phase at 275 K with different yields and different product selectivity [14–16,20]. The yields of these photo-formed N_2, O_2 and N_2O increased linearly with the UV-irradiation time and the reaction immediately ceased when irradiation was discontinued, as shown in Fig. 3, indicating that the presence of Ti-oxides included within the zeolites as well as the UV-irradiation light are indispensable for the photocatalytic reaction to take place, while the direct decomposition of NO to produce N_2, O_2 and N_2O occurs photocatalytically on the surface of the Ti-oxide single-site catalyst.

The photocatalytic reactivities of various Ti-oxide catalysts for the direct decomposition of NO are shown in Table 1. Of special interest is the comparison of the photocatalytic activities of the Ti-oxide/Y-zeolite catalysts with that of the widely used bulk TiO_2 powdered catalyst. It can be seen that the specific photocatalytic reactivities of the Ti-oxide/Y-zeolite catalysts, which have been normalized for the unit amount of TiO_2 in the catalysts, are much higher than that for the bulk TiO_2 catalysts [14–16,20].

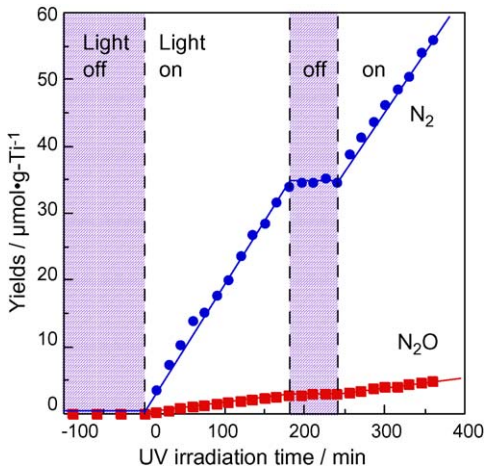

Fig. 3. The reaction–time profiles of the photocatalytic decomposition of NO into N_2 and N_2O on the ex-Ti-oxide/Y-zeolite.

Table 1
Yields of the photo-formed products, N_2 and N_2O in the photocatalytic decomposition of NO at 275 K and their distribution on various Ti-based photocatalysts.

Catalyst	Ti content (wt.% as TiO_2)	Yields (μmol/g of TiO_2 h)			Selectivity (%)	
		N_2	N_2O	Total	N_2	N_2O
ex-Ti-oxide/Y-zeolite	1.1	14	1	15	91	9
imp -Ti-oxide/Y-zeolite	1.0	7	10	17	41	59
imp-Ti-oxide/Y-zeolite	10	5	22	27	19	81
TiO_2 powder		2	6	8	25	75

Table 1 also shows the yields of the photo-formed N_2 and N_2O (efficiency) and their distribution (selectivity) in the photocatalytic decomposition of NO on various types of Ti-oxide catalysts. From Table 1, it is clear that the efficiency and selectivity for the formation of N_2 strongly depend on the type of catalyst. The ex-Ti-oxide/Y-zeolite catalyst exhibits a high reactivity and a high selectivity for the formation of N_2, while the formation of N_2O was found to be the major reaction on the bulk TiO_2 catalyst as well as on the imp-Ti-oxide/Y-zeolite catalyst. Thus, the results obtained with the ex-Ti-oxide/Y-zeolite clearly show the large difference in selectivity as well as efficiency with the imp-Ti-oxide/Y-zeolite and the bulk TiO_2 catalyst [14–16,20].

XAFS (XANES and EXAFS) investigations of Ti-oxide catalysts at the Ti K-edge were carried out and it was revealed that the Ti-oxide species has a tetrahedral coordination for the ex-Ti-oxide/Y-zeolite catalyst while, for the imp-Ti-oxide/Y-zeolite catalyst, the Ti-oxide species had a octahedral coordination. Moreover, the relationship between the coordination number of the Ti-oxide species and the selectivity for N_2 formation in the photocatalytic decomposition of NO on various types of Ti-oxide based photocatalysts are shown in Fig. 4. A clear dependence of the N_2 selectivity on the coordination number of the Ti-oxide species can be observed, i.e., the lower the coordination number of the Ti-oxide species, the higher the N_2 selectivity. From these results, it can be proposed that a highly efficient, highly selective photocatalytic reduction of NO into N_2 and O_2 can be achieved using the ex-Ti-oxide/Y-zeolite, which includes the highly dispersed isolated tetrahedral Ti-oxide as the active species. Also, the formation of N_2O as the major product was observed for the bulk TiO_2 catalysts and on the imp-Ti-oxide/Y-zeolite catalysts, which include the aggregated octahedrally coordinated Ti-oxide species.

Photoluminescence investigations of the ex-Ti-oxide/Y-zeolite catalyst were also carried out and a photoluminescence spectrum at around 490 nm by excitation at around 290 nm at 77 K due to the highly dispersed tetrahedrally coordinated Ti-oxide species was observed, as shown in Fig. 5. However, no photoluminescence spectrum could be observed for the imp-Ti-oxide/Y-zeolite catalysts. The addition of NO onto the ex-Ti-oxide/Y-zeolite catalyst led to an efficient quenching of the photoluminescence spectrum and the lifetime of the charge-transfer excited state was also found to be shortened, its extent depending on the amount of NO added. These results indicate not only that the tetrahedrally coordinated Ti-oxide species may be located at positions accessible to the added NO but also that the added NO easily interacts with the charge-transfer excited state of the species [14–16,20].

Based on these results, the reaction mechanism for the photocatalytic decomposition of NO on the isolated tetrahedral Ti-oxide species was proposed, as shown in Scheme 1. The NO species was able to adsorb onto these oxide species as weak ligands to form the reaction precursors. Under UV-irradiation, the charge-transfer excited complexes of the oxides, $(Ti^{3+}–O^-)^*$, are formed. Within their lifetimes, the electron transfer from the trapped electron center, Ti^{3+}, into the π-antibonding orbital of NO takes place and, simultaneously, the electron transfer from the π-bonding orbital of another NO into the trapped hole center, O^-, occurs. These electron transfers led to the direct decomposition of two sets of NO on $(Ti^{3+}–O^-)^*$ into N_2 and O_2 under UV-irradiation in the presence of NO even at 275 K. On the other hand, with the aggregated or bulk TiO_2 catalysts, the photo-formed holes and electrons rapidly separate from each other with large space distances between the holes and electrons, thus, preventing the simultaneous activation of two NO on the same active sites and resulting in the formation of N_2O and NO_2 in place of N_2 and O_2. Moreover, the decomposed N and O species react with NO on different sites to form N_2O and NO_2, respectively.

These results clearly demonstrate that zeolites used as supports enable the construction of the Ti-oxide species in a highly dispersed state within the zeolite cavities, thus, such tetrahedrally

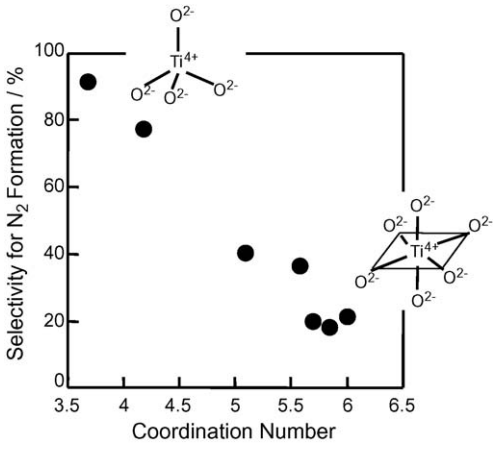

Fig. 4. Relationship between the coordination number of Ti-oxide species and the selectivity for N_2 formation in the photocatalytic decomposition of NO on various titanium oxide photocatalysts.

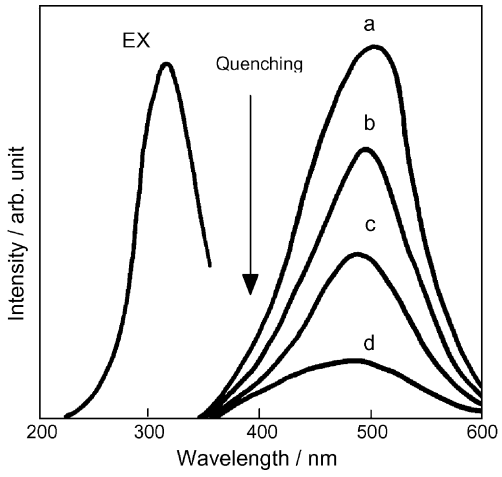

Fig. 5. The observed ordinary photoluminescence spectrum of the ex-Ti-oxide/Y-zeolite catalyst (a), its excitation spectrum (EX), and effects of the addition of CO_2 and H_2O (b, c) and the loading of Pt (d) on the photoluminescence spectrum at 77 K. Excitation at 290 nm, emission monitored at 490 nm, amounts of added CO_2: (b) 8.5, and H_2O; (c) 2.9 μmol g^{-1}.

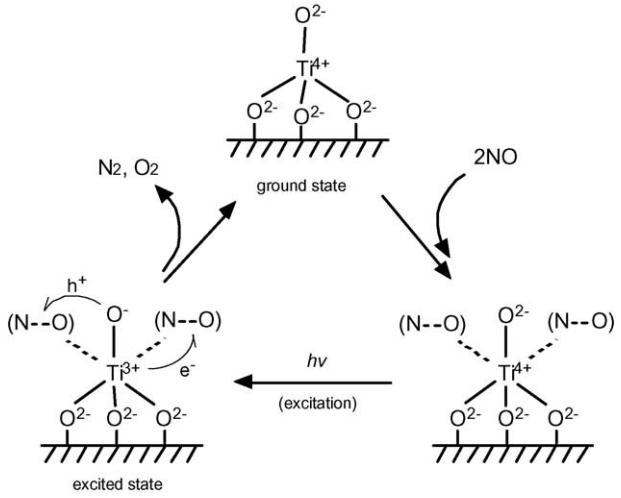

Scheme 1. Reaction scheme of the photocatalytic decomposition of NO into N_2 and O_2 on the Ti-oxide/Y-zeolite catalyst at 275 K.

coordinated Ti-oxide photocatalysts can be seen to be promising candidates for unique and applicable photocatalysts for the reduction of toxic NOx compounds.

2.3. Design of visible light-responsive Ti/zeolite catalysts by applying an advanced metal ion implantation method

Titanium oxide photocatalysts anchored within various zeolites exhibit unique and high photocatalytic activity, however, the isolated tetrahedral Ti-oxide species absorbs UV light of wavelengths below 300 nm. Photocatalysts which can operate efficiently under both UV and visible light are urgently required for practical and widespread use. A modification of the electronic properties of Ti/zeolite photocatalysts by bombarding them with high-energy metal ions has led to the discovery that metal ion-implantation with various transition-metal ions such as V or Cr accelerated by high electric fields can produce a large shift in the absorption band toward visible light regions [10]. Ti-HMS and Ti-MCM-41 exhibit their absorption spectra at around 200–260 nm which can be attributed to the charge-transfer absorption process involving an electron transfer from the O^{2-} to Ti^{4+} ion of the highly dispersed tetrahedrally coordinated Ti-oxide species of these catalysts [10]. However, V ion-implantation on Ti-HMS and Ti-MCM-41 lead to a large shift in their absorption spectra toward visible light regions, the extent strongly depending on the amount of V ions implanted. These results indicate that the interaction of the implanted V ions with the tetrahedrally coordinated Ti-oxide species lead to a modification of the electronic properties of the Ti-oxide species within the zeolite framework, enabling them to absorb visible light. The photocatalytic activity of the V ion-implanted Ti-HMS and Ti-MCM-41 was also investigated for the decomposition of NO into N_2 and O_2 under visible light irradiation ($\lambda > 420$ nm). Visible light irradiation of the V ion-implanted Ti-HMS led to the efficient decomposition of NO into N_2 and O_2, while the unimplanted original Ti-HMS exhibited no activity for the reaction under the same conditions [10]. These results show that ion-implantation is an effective technique for the modification of the electronic properties of titanium oxide photocatalysts, enabling them to absorb and operate under visible light ($\lambda > 420$ nm) with high efficiency.

The local environment of the implanted metal ions was investigated by XANES and EXAFS (XAFS) analyses [10]. The V K-edge FT-EXAFS spectra of the Ti-HMS catalyst implanted with V ions show that the next-neighbors of the V environment are not the same as the vanadium-oxide based catalysts (e.g., V_2O_5) and suggest the formation of tetrahedral titanium oxides having a V–O–Ti bond instead of V–O–V linkage [10]. These findings show that the formation of the V–O–Ti bridge structures between the isolated tetrahedrally coordinated Ti-oxide species and implanted V ions affect the electronic structure of the isolated Ti-oxide species, leading to a red shift in the absorption spectra of these catalysts.

It has also been recently reported that the Ti^{4+}–O–Ce^{3+} linkage constructed within MCM-41 (Ti/Ce-MCM-41) exhibits photocatalytic activity for the oxidation of 2-propanol into acetone or CO_2 under visible light irradiation ($\lambda = 460$ nm) [38]. The Ti^{4+}–O–Ce^{3+} linkage was constructed within MCM-41 by the reaction between an isolated $(OH)Ti(OSi)_3$ site and $Ce(III)NO_3$ in acetonitrile. Ti-MCM-41 and Ce-MCM-41 exhibit no absorption bands in the visible light region, while Ti/Ce-MCM-41 absorbs visible light up to 540 nm. Ce L_{III}-edge XANES investigations strongly suggest that the Ce ions exist in trivalent state within Ti/Ce-MCM-41. Considering these XANES results, the visible light absorption of Ti/Ce-MCM-41 may be considered to be due to the metal-to-metal charge-transfer (MMCT) excitation of the Ti^{4+}–O–Ce^{3+} linkage (Ti^{4+}–O–$Ce^{3+} \rightarrow Ti^{3+}$–O–$Ce^{4+}$) which plays an important role in the oxidation of 2-propanol [38].

3. Photocatalytic reactions on V-oxide species constructed within zeolite framework structures

Zeolites having transition metal oxides in their frameworks have been the focus of much attention for their interesting and distinctive properties. So far, several types of zeolites incorporating V-oxide species have been developed and the true chemical nature and reactivity of the species, especially their photochemical properties, are beginning to be understood. Among these, the unique photocatalytic properties of the V-oxide species towards the partial oxidation of alkenes as well as other reactions have been reported [21–25,39]. In fact, the dispersion level of the V-oxide species is known to be the key factor in controlling the photocatalytic reactivity and a well-prepared V-oxide species within a zeolite framework structure has been shown to exhibit unique and high photocatalytic reactivity.

The VS-1 catalyst exhibited a photoluminescence spectrum having a vibrational fine structure at around 400–650 nm upon excitation at around 300 nm due to the highly dispersed tetrahedrally coordinated V–O moieties in C_{3v} symmetry [21–25]. Those excitation and photoluminescence spectra are attributed to the charge-transfer processes on the V–O moieties of the tetrahedral vanadate ions (VO_4^{3-}), involving an electron transfer from the O^{2-} to V^{5+} ions and a reverse radiative decay from the charge-transfer excited triplet state to its ground state:

$$(V^{5+} = O^{2-}) \underset{h\nu'}{\overset{h\nu}{\rightleftarrows}} (V^{4+}-O^{-})^{*}$$

From the second derivative of the photoluminescence spectrum, the energy separation between the (0–0) and (0–1) vibrational transitions was determined to be about 960 cm^{-1} and was attributed to the vibrational transition in the V=O bond. An energy separation of 960 cm^{-1}, obtained from the photoluminescence spectrum of VS-1, was found to be slightly different from that of the V-oxide species highly dispersed on silica (1035 cm^{-1}) [21–25,40,41]. The V=O bond length of the V–O moieties within the zeolite framework structure of VS-1 obtained from the curve-fitting results of FT-EXAFS was 1.68 Å. The V=O bond length (1.68 Å) was found to be longer than that of the V–O moieties anchored on the surface of Vycor glass or silica (1.62 Å), showing that the O=V–O(Si) bond angle was smaller for the V–O moieties within the zeolite framework structure [21–25,40,41]. These results indicate that a highly dispersed V-oxide species is

present within the zeolite framework as a tetrahedrally coordinated species and that the charge-transfer excited state of this oxide species is well localized in the shorter V=O bond. The addition of propane or NO onto VS-1 led to the efficient quenching of the photoluminescence as well as a shortening of the photoluminescence lifetime, indicating that propane or NO interacts with the excited state of the V–O moieties so that the catalyst might act as a photocatalyst for reactions with NO or propane [21–25]. The reaction–time profile of the yields of N_2 in the photocatalytic decomposition of NO in the absence and the presence of propane on the VS-1 catalyst is shown in Fig. 6. UV-irradiation of the catalyst in the presence of NO leads to the photocatalytic decomposition of NO while the evolution of N_2 is also observed together with O_2 and N_2O as minor products. The reaction proceeds much more efficiently under a mixture of NO and propane, thus, leading to the formation of propylene, ethylene and oxygen-containing compounds such as CH_3CHO and CO_2 in addition to the evolution of N_2. The yield as well as the selectivity for the formation of N_2 increased in proportion to the amount of added propane, while the yield of the formation of N_2O decreased and the yield of the oxygen-containing products increased [21–25]. Moreover, the turnover frequency of the catalyst for the decomposition of NO exceeded unity after prolonged UV-irradiation. These results clearly indicate that this reaction proceeds photocatalytically and that the photocatalytic reduction of NO could proceed efficiently in the presence of propane on the VS-1 catalyst. The reduction of NO with propane on VS-1 was about five times higher than on the V-oxide photocatalyst anchored onto porous Vycor glass or silica, indicating that the difference in the coordination structure and electronically excited states of the V-oxide species are the main factors controlling the reactivity for the photocatalytic reduction of NO. The efficiency of the photocatalytic reduction of NO was found to depend strongly on the kind of hydrocarbons used, such as CH_4 and C_2H_6, and among these hydrocarbons, C_3H_8 showed the highest enhancement in the reaction rate, indicating that the abstraction of the H atom from the hydrocarbons by a charge-transfer excited state, $(V^{4+}–O^-)^*$, plays a significant role in the enhancement of the reaction [21–25]. The importance of the abstraction of an H atom from the hydrocarbons is also confirmed by the fact that the presence of CO did not enhance the photocatalytic reduction of NO. The photo-induced adsorption of NO and C_3H_8 were also investigated. Only small amounts of NO were found to be adsorbed onto the catalyst under UV-irradiation while the adsorption of NO was greatly enhanced in the co-existence of C_3H_8. These results suggest the importance of the intermediate species formed from NO and hydrocarbon-radicals, followed by further reactions with NO to produce N_2 as well as oxygen-containing products such as CH_3CHO and CO_2. From these results, it can be emphasized that the differences in the coordination structures and the electronically excited states of the V-oxide species are the main factors controlling the photocatalytic activity for the direct decomposition as well as reduction of NO. The incorporation of a V-oxide species into the zeolite framework made it possible to control the local structure as well as the electronic state of the V-oxide species on a molecular scale. Thus, using zeolites as host materials for active sites in various photocatalytic reactions can be considered an especially promising way to develop unique and well-defined photocatalysts having high reactivity and selectivity.

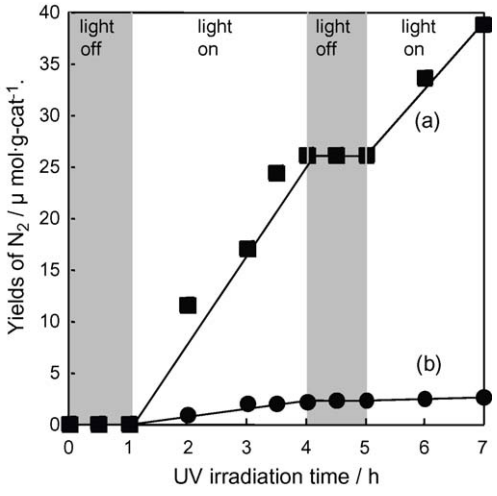

Fig. 6. Reaction–time profiles of the photocatalytic decomposition of NO (a) with and (b) without propane on VS-1. Propane added: 1.97×10^{-4} mol/g-cat, NO: 1.82×10^{-4} mol/g-cat.

The highly dispersed V-oxide species exhibit unique photocatalytic activity, however, UV light irradiation is essential for their activation. It has been reported that the alkali-ion modification of the highly dispersed V-oxide species results in the formation of a unique surface vanadate species which exhibits photocatalytic activity for the partial oxidation of hydrocarbons under visible light irradiation ($\lambda > 390$ nm) [42,43]. The V/SiO_2 (VS) catalyst prepared by an impregnation method exhibits a typical photoluminescence spectrum at around 500 nm with a well-defined vibrational fine structure upon excitation at 310 nm due to the highly dispersed tetrahedrally coordinated V-oxide species. However, the addition of alkali metal ions such as Na^+, K^+ and Rb^+ onto the VS catalyst by an impregnation method (Na_2O–VS, K_2O–VS, Rb_2O–VS) led to the appearance of unique featureless photoluminescence at around 530 nm upon excitation at 400 nm. This featureless photoluminescence can be attributed to the formation of the VO_4 tetrahedron where two V–O bonds interact with an alkali metal ion [43]. This unique V-oxide species exhibits photocatalytic activity for the partial oxidation of hydrocarbons under visible light irradiation ($\lambda > 390$ nm), e.g., Rb_2O–VS oxidizes propane into COx (CO and CO_2) and propanone photocatalytically. The conversion of propane reached 67.1%, while the selectivity for COx (CO and CO_2) and propanone were 34% and 60%, respectively [43].

Another type of visible light-responsive photocatalyst has recently been prepared by the isomorphous substitution of a Ti^{4+} species within ETS-10 with the V-oxide species [44]. ETS-10 is a microporous titanosilicate zeolite with a framework containing linear Ti–O–Ti–O– chains where Ti^{4+} species exist in octahedral coordination. The vanadium substituted ETS-10 (ETVS-10: V/(V + Ti) = 0.43) was prepared by hydrothermal treatment. The Raman spectrum of ETVS-10 shows a characteristic –V–O–Ti– bond vibration at 839 cm^{-1} while the NEXAFS spectrum of ETVS-10 exhibits peaks due to the L_{III}- and L_{II}-edges of V^{5+} and V^{4+}, clearly suggesting the isomorphous substitution of the Ti^{4+} species with the V^{5+} and V^{4+} species [44]. The band gap energy of ETS-10 decreased from 4.32 to 3.58 eV by the isomorphous incorporation of the V species, enabling the absorption of visible light above 400 nm. In fact, ETVS-10 exhibited photocatalytic activity for the polymerization of ethylene under visible light irradiation ($\lambda > 400$ nm) [44].

4. Photocatalytic reactions on Mo-MCM-41 catalyst

Mo-MCM-41 (1.0 Mo wt.%) exhibited photoluminescence at around 400-600 nm upon excitation at around 295 nm (defined as X), coinciding with the photoluminescence of the tetrahedrally coordinated Mo-oxide species highly dispersed on SiO_2. Those excitation and emission spectra are attributed to the charge-transfer processes on the Mo–O moieties of the isolated tetrahedral molybdate ions (MoO_4^{2-}), involving an electron transfer from the

O^{2-} to Mo^{6+} ions and a reverse radiative decay from the charge-transfer excited triplet state. The width and wavelength at the maximum intensity of the emission band did not change upon varying the excitation wavelength, indicating that there is only one luminescent moiety.

$$[Mo^{6+}=O^{2-}] \xrightarrow{h\nu} [Mo^{5+}=O^{-}]^{*} \xrightarrow{h\nu'} [Mo^{6+}=O^{2-}]$$

On the other hand, there were at least two luminescent species (absorption spectrum can be deconvoluted into two components in wavelength regions X and Y: 295 and 310 nm, respectively) on Mo-MCM-41 (4.0 Mo wt.%) [28]. The increase in the Mo content led to the formation of not only an emitted X site with a photoluminescence lifetime of 2.25 ms but also another emitting Y site with low photoluminescence yields and a short photoluminescence lifetime (0.91 ms). Taking the results of XAFS measurements into consideration, only isolated tetrahedrally coordinated Mo-oxides are formed at lower Mo loadings, while isolated tetrahedrally coordinated Mo-oxides as well as an oligomeric tetrahedral $(MoO_4^{2-})_n$ species are formed in higher Mo loadings. The addition of C_3H_8 or NO to Mo-MCM-41 (1.0 Mo wt.%) was seen to lead to the efficient quenching of the photoluminescence as well as a shortening of the photoluminescence lifetime, as shown in Fig. 7. On the other hand, as shown in Fig. 8, for Mo-MCM-41 (4.0 Mo wt.%), NO or C_3H_8 interacted with the X site more efficiently than the Y site. It can, thus, be expected that an isolated tetrahedral Mo-oxide species will exhibit higher photocatalytic reactivity as compared to the $(MoO_4^{2-})_n$ species.

Measurements on the photocatalytic reaction of NO in the presence of C_3H_8 were performed on Mo-MCM-41. Under UV-irradiation, the photocatalytic reaction of NO with C_3H_8 was found to proceed efficiently, leading to the formation of N_2 and oxygen-containing compounds such as CH_3COCH_3 and CO_2. Fig. 9 shows the relationship between the yields of N_2, or CH_3COCH_3 formation and relative intensity of the absorption spectra observed in the region of 295 nm for Mo-MCM-41 (0.5, 1.0, 2.0 and 4.0 Mo wt.%). The intensities of the absorption spectra at 295 nm have a good relationship with the yields of N_2 or CH_3COCH_3 formation, suggesting that the charge-transfer excited triplet state of the tetrahedrally coordinated Mo-oxide species in a highly dispersed state plays a significant role in the reaction.

After UV-irradiation of Mo-MCM-41 in the presence of C_3H_8, its subsequent evacuation at 295 K did not lead to the recovery of the original photoluminescence intensity but to the appearance of the ESR signals due to Mo^{5+} ions.

This shows that the charge-transfer excited triplet state of the Mo-oxide species abstracts the H atom from C_3H_8 to form a Mo^{5+} ion and hydrocarbon radical [28]. Moreover, only small amounts of NO or C_3H_8 were photoadsorbed under UV-irradiation; however, a great enhancement of the photoadsorption occurred in the presence of a mixture of NO and C_3H_8. Based on these considerations, the following reaction mechanism can be proposed: the intermediate species formed between NO and the hydrocarbon radicals, which is formed by H abstraction of the photo-excited Mo-oxide species from C_3H_7, subsequently reacts with NO to produce N_2 as well as oxygen-containing compounds.

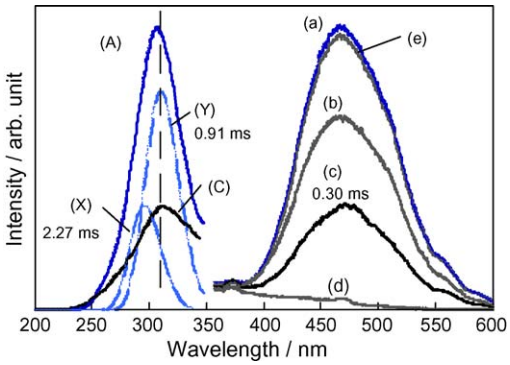

Fig. 8. Effect of the addition of NO on the photoluminescence spectrum and its excitation spectrum of the Mo-MCM-41 (4.0 Mo wt.%). Pressure of added NO: (A, a) 0, (b) 0.6, (C, c) 4 Torr, (d) excess, (e) degassed after (d). Spectrum (A) can be deconvoluted into (X) and (Y).

It was also found that the photocatalytic decomposition reactions of NO were dramatically enhanced in the presence of CO, leading to the formation of N_2 and CO_2. Fig. 10 shows the relationship between the yields of N_2 formation for the decomposition of NO on Mo-MCM-41 (0.5–4.0 Mo wt.%) in the presence of CO and the relative intensity of the absorption spectra observed in the total region (X and Y) of the catalyst. The yields of N_2 have a good relationship with the intensities of the absorption spectra in the total region of X and Y as well as with the amount of Mo^{4+} ions generated through the photoreduction of Mo^{6+} with CO (number of Mo^{4+} ions estimated by the number of photo-formed CO_2 molecules) [28,45]. These results indicate that the charge-transfer excited triplet states of both the isolated tetrahedral Mo-oxides and $(MoO_4^{2-})_n$ play a significant role in the reaction.

UV-irradiation of Mo-MCM-41 in the presence of CO alone and its subsequent evacuation at 293 K led to an efficient quenching of the photoluminescence. However, under identical conditions, no ESR signals due to the Mo^{5+} ions were detected, suggesting that the charge-transfer excited triplet state, i.e., the $[Mo^{5+}–O^{-}]^{*}$ complex reacts with CO to form Mo^{4+} ions and CO_2. It was found that the Mo^{4+} ions formed reacts efficiently with NO and N_2O under dark conditions to produce N_2O and N_2, respectively, as well as for the reoxidation of Mo^{4+} to Mo^{6+} ions, indicated by the reappearance of

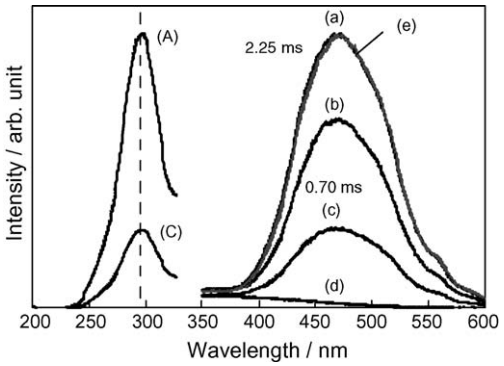

Fig. 7. Effect of the addition of NO on the photoluminescence spectrum and its excitation spectrum of the Mo-MCM-41 (1.0 Mo wt.%). Pressure of added NO: (A, a) 0, (b) 0.07, (C, c) 0.4 Torr, (d) excess, (e) degassed after (d).

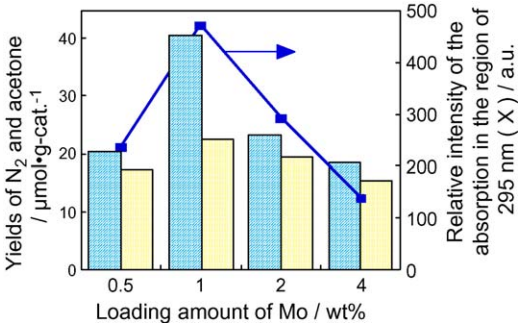

Fig. 9. Relationship among the yields of N_2 (left), acetone (right) formation and the relative intensity of the absorption in the region of 295 nm (X) calculated by the deconvolution of the original excitation spectrum of the Mo-MCM-41 (0.5, 1.0, 2.0, and 4.0 Mo wt.%). Added propane or NO: 180 μmol g-cat.$^{-1}$.

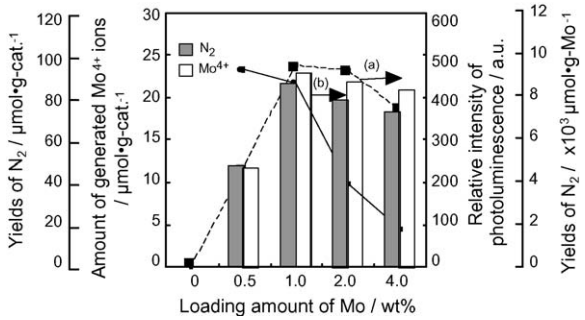

Fig. 10. Relationships between the yields of N_2 formation for the photocatalytic decomposition reactions of NO by the coexistence of CO (left), amount of generated Mo^{4+} ions, the relative intensity of the absorption in the total region of (X and Y) (dotted line; a) and the yields of N_2 per Mo atoms of 1 g (solid line; b) of Mo-MCM-41 (0.5, 1.0, 2.0, and 4.0 Mo wt.%). Added NO or CO: 180 μmol g-cat.$^{-1}$.

the photoluminescence of Mo^{6+} ions after the addition of NO and N_2O. From these results, it could be concluded that the following catalytic cycle plays a major role in the photocatalytic decomposition of NO in the presence of CO, i.e., Mo^{4+} ions that are formed through the reaction of the charge-transfer excited triplet state of $Mo^{6+}{=}O^{2-}$ with CO are reoxidized back to the original Mo^{6+} species in the presence of NO or N_2O.

So far as the photo-oxidation of CO by O_2 is concerned – an important reaction in fuel cell technology since it is essential to remove CO impurities from H_2 otherwise electrode performance is poisoned – we are again led to a plausible mechanism (Fig. 11) based on the known structures, as determined by XAFS, of the single-site $Mo^{6+}O_4$ centre [29,30]. Again a charge-transfer excited triplet state is implicated (and observed), and good quantum yields are obtained. This single-site photocatalytic method of purifying H_2 from its unwanted CO impurity is an alternative to the thermally activated heterogeneous catalytic method of achieving the same end using a Pt–Fe and other noble-metal catalysts supported on alumina [46].

5. Photocatalytic reactions on Cr-HMS and Cr-MCM-41 catalysts

We have found that the Cr-containing mesoporous zeolite (Cr-HMS) shows photocatalytic reactivity for the photocatalytic decomposition of NO into N_2 and O_2 and the partial oxidation of C_3H_8 with O_2 under both UV and visible light (or sunlight) irradiation. Here, special attention is focused on an understanding of the local structure of the Cr-oxide species on Cr-HMS and their photocatalytic activity for NO decomposition [31].

The UV–vis spectra of the Cr-HMS catalysts exhibited three distinct absorption bands at around 250, 360 and 480 nm which could be assigned to the charge-transfer from O^{2-} to Cr^{6+} of the tetrahedrally coordinated Cr-oxide species, as shown in Fig. 12 [31,47]. Absorption bands above 550 nm assigned to the dichromate or Cr_2O_3 cluster could not be observed, indicating that the tetrahedrally coordinated Cr-oxide species exists in an isolated state. Cr-HMS exhibited photoluminescence spectra at ca. 550–750 nm upon excitation of the absorption (excitation) bands at ca. 250, 360 and 480 nm. These absorption and photoluminescence spectra are similar to those obtained with well-defined, highly dispersed Cr-oxides anchored onto Vycor glass or silica

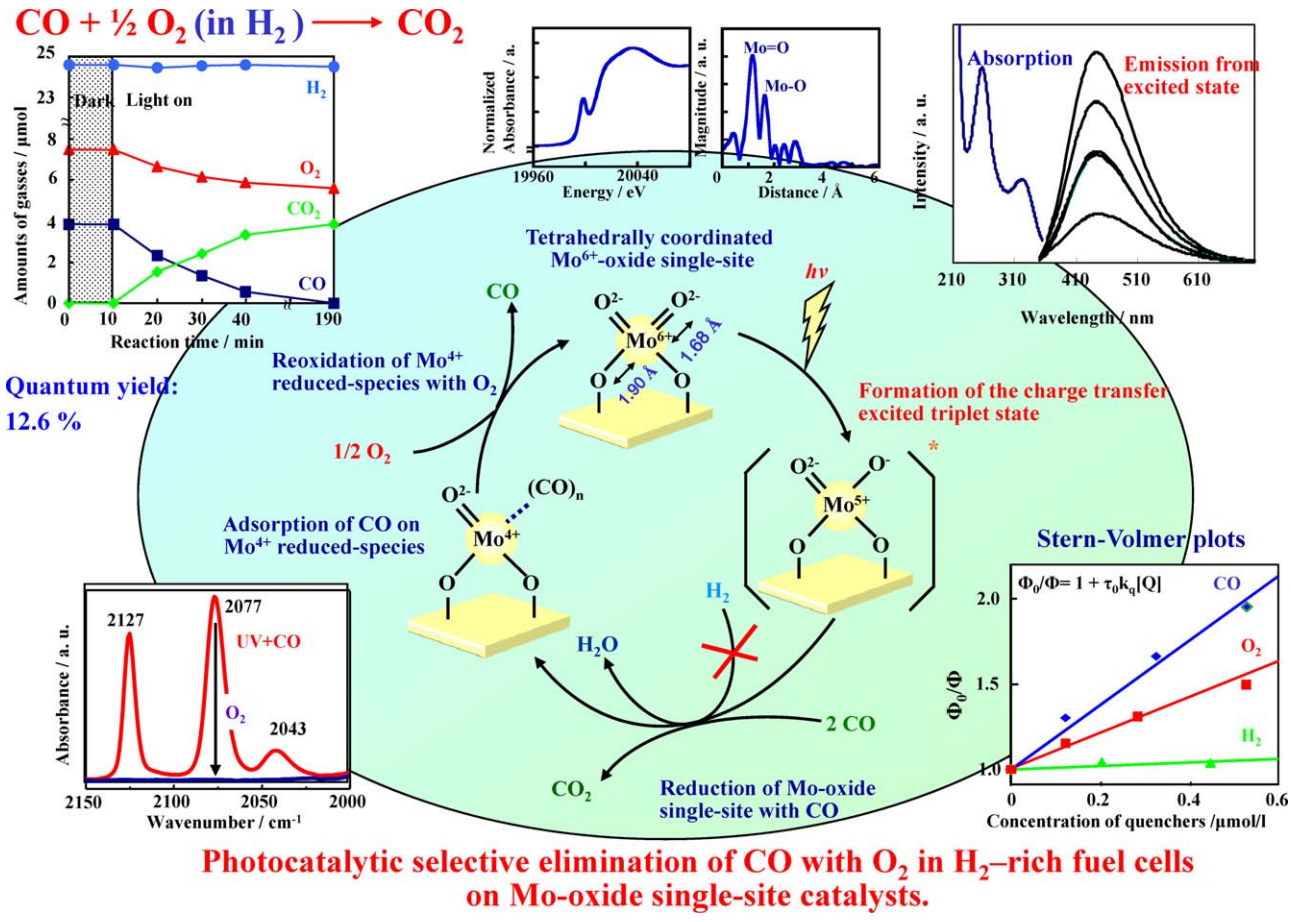

Fig. 11. Photocatalytic selective elimination of CO with O_2 in the presence of H_2 on single-site Mo-oxide catalysts.

[15,16,31,47] and can be attributed to charge-transfer processes on tetrahedrally coordinated Cr-oxide species involving an electron transfer from O^{2-} to Cr^{6+} and a reverse radiative decay, respectively.

UV-light irradiation ($\lambda > 270$ nm) of Cr-HMS in the presence of NO in the gas phase at 275 K led to the photocatalytic decomposition of NO and the evolution of N_2, N_2O and O_2. Cr-HMS also showed photocatalytic reactivity even under visible light irradiation ($\lambda > 450$ nm). The N_2 yields increased linearly with the irradiation time and the reaction stopped immediately when irradiation was ceased, as shown in Fig. 13. After prolonged irradiation, the amount of decomposed NO to form N_2 per total number of Cr ions included within the catalyst exceeded unity. These results clearly indicate that the presence of both the Cr-oxide species as well as light irradiation are indispensable for the photocatalytic reaction to proceed and that the direct decomposition of NO occurs photocatalytically. Although the reaction rate under visible light was less than that under UV-light irradiation, the selectivity for N_2 formation (97%) under visible light was higher than that with UV-irradiation (45%). These results indicate that Cr-HMS can absorb and act as an efficient photocatalyst not only under UV but also visible light irradiation, significantly, to form N_2. The addition of NO to the Cr-HMS catalyst led to an efficient quenching of the photoluminescence spectrum, indicating that the charge-transfer excited state of the tetrahedrally coordinated isolated Cr-oxide species, $(Cr^{5+}–O^{-})^*$, can easily interact with NO and also that the photo-excited species plays a major role in the photocatalytic reaction under UV and visible light irradiation.

The popular, proton exchange membrane (PEM) fuel cells, also designated polymer electrolyte fuel cells (PEFC), demand a supply of H_2 stringently free of CO impurity, and the favoured method of achieving this is to catalytically oxidize the CO over either a transition-metal oxide or, preferably, a supported Pt-rich catalyst, known generally as PROX (preferential oxidation of CO in the presence of H_2)[48–50]. But in view both of the continuing high cost and ultimate scarcity of Pt, it is highly desirable to design a PROX catalyst for static fuel cell installations that is not only cheap and readily preparable but also function at ambient temperatures. Here, it will be reported that Cr^{6+} ions function as a photocatalytic system under visible (or solar light) irradiation, thereby affording a clean, convenient (non-precious metal) catalyst for the PROX system. The XANES spectrum of Cr^{6+}-MCM-41 showed an intense and characteristic pre-edge peak, indicating that Cr^{6+}-MCM-41 contains a Cr^{6+}-oxide species in tetrahedral coordination, as can be seen in Fig. 14 [32]. Curve-fitting analysis of the Cr–O peaks revealed that the Cr^{6+}-oxide species exists in a highly distorted tetrahedral coordination with two shorter Cr=O double bonds (bond length (R) = 1.59 Å, coordination number of CN = 2.0) and two longer Cr–O single bonds (R = 1.85 Å, CN = 2.1). UV–vis spectrum of Cr^{6+}-MCM-41 exhibits three distinct absorption bands

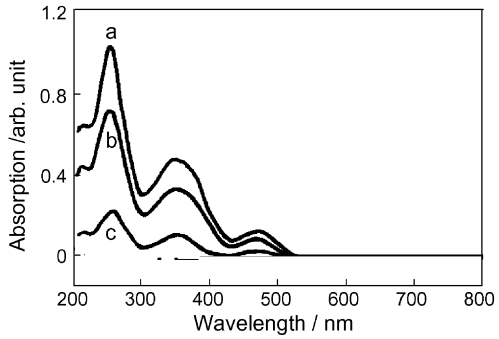

Fig. 12. UV–vis spectra of Cr-HMS catalysts (a) 2.0 wt.%, (b) 1.0 wt.%, (c) 0.2 wt.%, as Cr.

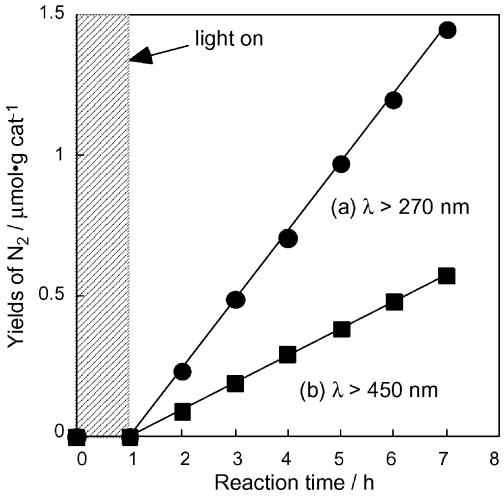

Fig. 13. The reaction–time profile of N_2 formation in the photocatalytic decomposition of NO on the Cr-HMS catalyst at 273 K (2.0 wt.% as Cr) under UV-light irradiation (a: $\lambda > 270$ nm) and visible light irradiation (b: $\lambda > 450$ nm).

at around 240, 350 and 460 nm due to the ligand to metal charge-transfer transition (LMCT: from O^{2-} to Cr^{6+}) of the tetrahedrally coordinated Cr^{6+}-oxide species [31,32,51]. Cr^{6+}-MCM-41 exhibited a photoluminescence spectrum at around 550–800 nm upon excitation at around 240, 350 and 460 nm at 298 K, due to the tetrahedrally coordinated Cr^{6+}-oxide species. The absorption and emission spectra are attributed to the following charge-transfer processes on the Cr=O moieties of the tetrahedral monochromate species (CrO_4^{2-}) involving an electron transfer from O^{2-} to Cr^{6+} ions and a reverse radiative decay from the charge-transfer excited triplet state [31,47,52]:

$$[Cr^{6+} = O^{2-}] \xrightarrow{h\nu} [Cr^{5+} - O^{-}]^* \xrightarrow{h\nu'} [Cr^{6+} = O^{2-}]$$

The photoluminescence of Cr^{6+}-MCM-41 is quenched in its intensity by the addition of CO, O_2 and H_2, indicating that the Cr^{6+}-oxide species, in its charge-transfer excited triplet state, easily interacts with CO, O_2 and H_2. Moreover, the absolute quenching rate constants (k_q (l/mol s)) for each gas which were determined by the Stern–Volmer plots [32,53], were found to increase in the following order: H_2 $(8.63 \times 10^5) \ll$ CO $(5.91 \times 10^9) < O_2$ (1.12×10^{10}). These results indicated that CO interacts very efficiently with the photo-excited Cr^{6+}-oxide species as compared to H_2. Fieldwork experiments were carried out to investigate the photocatalytic reactivity of Cr^{6+}-MCM-41 for the preferential oxidation of CO with O_2 in the presence of H_2 under natural conditions of clean and safe solar light irradiation. The reaction–time profiles of the photocatalytic oxidation of CO with O_2 in the presence of H_2 on Cr^{6+}-MCM-41 under solar light are shown in Fig. 14. These data were observed from 11:00 to 14:30 of a sunny day with average solar light intensity of 78.5 mW/cm^2 and irradiation area of 3 cm^2, clearly showing that Cr^{6+}-MCM-41 could operate efficiently as a photocatalyst for CO oxidation. After light irradiation for 3.5 h, CO conversion and selectivity reached ~100% and 96%, respectively. The present results demonstrated that Cr^{6+}-MCM-41 can be applied for clean and cost-efficient photo-PROX reaction systems using solar light energy at ambient temperatures without the use of Pt or other precious noble metals.

As shown in Fig. 14, visible light irradiation of Cr^{6+}-MCM-41 in the presence of CO led to the appearance of a typical FT-IR band due to the monocarbonyl Cr^{4+} species $[Cr^{4+}(CO)]$ at 2201 cm^{-1} [32], accompanied by the formation of CO_2. Moreover, the addition of O_2 on this system at 298 K led to the complete disappearance of FT-IR band, indicating the regeneration of the original Cr^{6+}-oxide species.

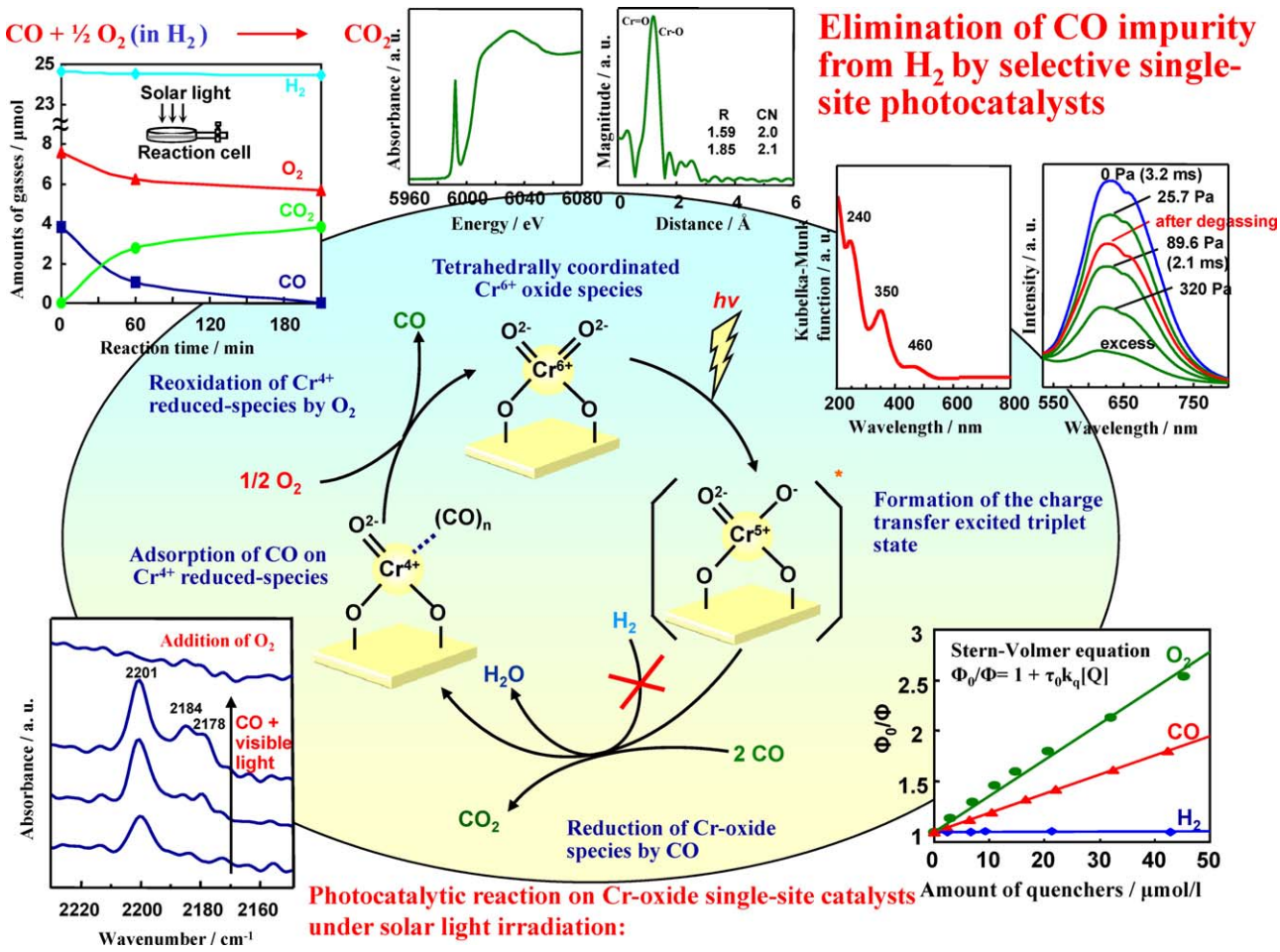

Fig. 14. Photocatalytic selective elimination of CO with O_2 in the presence of H_2 on single-site Cr-MCM-41 catalyst.

The catalytic reaction cycles on Cr^{6+}-MCM-41 under visible light ($\lambda > 420$ nm) or solar light irradiation can be proposed as in Fig. 14. That is, initially, the tetrahedral Cr^{6+}-oxide species is photo-excited to its charge-transfer excited triplet state and reacts with CO to form CO_2 and a photo-reduced Cr^{4+}-oxide species. Then the Cr^{4+}-oxide species are efficiently oxidized by O_2 and the original Cr^{6+}-oxide species are generated. The high CO selectivity observed for the Cr^{6+}-MCM-41 can be attributed to the high and selective reactivity of the photo-excited Cr^{6+}-oxide species with CO, as indicated by the high quenching efficiency of CO as compared to H_2.

These results show that the design of transition metal ion-containing zeolite catalysts is one of the most promising ways to develop unique light driven photocatalytic systems that enable the efficient utilization of abundant visible or solar light energy.

6. Conclusions

In this article, the photocatalytic reactivities of various transition metal oxides (Ti, V, Mo and Cr) incorporated within zeolite framework structures as single site heterogeneous catalysts were summarized. The interactions of these active species with gaseous NOx (NO and N_2O) and CO_2 were monitored and the photocatalytic reactivity of the catalysts for the decomposition of NOx as well as the reduction of CO_2 with H_2O has been presented.

Metal oxide catalysts (Ti, V, Mo and Cr) constructed within the framework or cavities of various zeolites by ion-exchange or hydrothermal synthesis were found to exist in highly dispersed tetrahedral coordination states and were observed to act as efficient photocatalysts for the decomposition of NO into N_2 and O_2 as well as the reduction of CO_2 with H_2O to produce CH_4 and CH_3OH. Photoluminescence investigations revealed that the efficient interaction of the charge-transfer photo-excited complexes of these oxides, $(Me^{(n-1)+}–O^{-})^*$, i.e., the electron–hole pair state with reactant molecules such as NO, CO_2 and H_2O, plays a significant role in the photocatalytic reactions.

From these results, it was shown that by utilizing the physicochemical properties of various zeolites such as the pore size diameter or the channel structure, it becomes possible to control the photocatalytic activity as well as the selectivity of the reaction, as was well demonstrated in the results of the photocatalytic reduction of CO_2 with H_2O on Ti-containing mesoporous zeolites. It can, thus, be seen that the use of zeolites is one of the most promising approaches in the design of efficient local structures at the molecular level for the development of effective photocatalytic systems to reduce and eliminate global air and water pollution.

References

[1] M. Anpo, in: P. Tundo, P. Anastas (Eds.), Green Chemistry, Oxford University Press, 2000, p. 1.
[2] M. Anpo, in: A. Corma, F.V. Melo, S. Mendioroz, J.L.G. Fierro (Eds.), Studies in Surface Science and Catalysis, vol. 130A, Proceedings of the 12th International Congress Catalysts, Granada, 2000, p. 157.
[3] D.F. Ollis, H. AlEkabi (Eds.), Photocatalytic Purification and Treatment of Water and Air, Elsevier, 1993.
[4] E. Pelizzetti, M. Schiavello (Eds.), Photochemical Conversion and Storage of Solar Energy, Kluwer Academic Publishers, 1991.
[5] M. Kitano, M. Matsuoka, M. Ueshima, M. Anpo, Appl. Catal. A: Gen. 325 (2007) 1.

[6] M. Kitano, M. Takeuchi, M. Matsuoka, J.M. Thomas, M. Anpo, Catal. Today 120 (2007) 133.
[7] M. Matsuoka, M. Anpo, Curr. Opin. Solid State Mater. Sci. 7 (2003) 451.
[8] M. Anpo, M. Che, Adv. Catal. 44 (2000) 119.
[9] M. Anpo, M. Takeuchi, K. Ikeue, S. Dohshi, Curr. Opin. Solid State Mater. Sci. 6 (2002) 381.
[10] M. Anpo, M. Takeuchi, J. Catal. 216 (2003) 505.
[11] H. Yamashita, M. Anpo, Curr. Opin. Solid State Mater. Sci. 7 (2003) 471.
[12] M. Anpo, Bull. Chem. Soc. Jpn. 77 (2004) 1427.
[13] M. Anpo, S. Dohshi, M. Kitano, Y. Hu, M. Takeuchi, M. Matsuoka, Ann. Rev. Mater. Res. 35 (2005) 1.
[14] M. Anpo (Ed.), Surface Photochemistry, Wiley, 1996 (and references therein).
[15] M. Anpo (Ed.), Photofunctional Zeolites, NOVA Publishers Inc., 2000 (and references therein).
[16] M. Matsuoka, M. Anpo, J. Photochem. Photobiol. C: Photochem. Rev. 3 (2003) 225.
[17] M. Anpo, H. Yamashita, Y. Ichihashi, Y. Fujii, M. Honda, J. Phys. Chem. 101 (1997) 2632.
[18] H. Yamashita, K. Ikeue, T. Takewaki, M. Anpo, Top. Catal. 18 (2002) 95.
[19] K. Ikeue, H. Yamashita, M. Anpo, Electrochemistry 70 (2002) 402.
[20] H. Yamashita, Y. Ichihashi, M. Anpo, M. Hashimoto, C. Louis, M. Che, J. Phys. Chem. 100 (1996) 16041.
[21] S. Higashimoto, M. Matsuoka, H. Yamashita, M. Anpo, Jpn. J. Appl. Phys. 38 (1999) 47.
[22] S. Higashimoto, M. Matsuoka, H. Yamashita, M. Anpo, O. Kitao, H. Hidaka, M. Che, E. Giamello, J. Phys. Chem. B 104 (2000) 10288.
[23] M. Anpo, S. Higashimoto, M. Matsuoka, N. Zhanpeisov, Y. Shioya, S. Dzwigaj, M. Che, Catal. Today 78 (2003) 211.
[24] Y. Hu, S. Higashimoto, S. Takahashi, Y. Nagai, M. Anpo, Catal. Lett. 100 (2005) 35.
[25] Y. Hu, N. Wada, K. Tsujimaru, M. Anpo, Catal. Today 120 (2007) 139.
[26] R. Tsumura, S. Higashimoto, M. Matsuoka, H. Yamashita, M. Che, M. Anpo, Catal. Lett. 68 (2000) 101.
[27] M. Matsuoka, T. Kamegawa, R. Takeuchi, M. Anpo, Catal. Today 122 (2007) 39.
[28] S. Higashimoto, Y. Hu, R. Tsumura, K. Iino, M. Matsuoka, H. Yamashita, Y.G. Shul, M. Che, M. Anpo, J. Catal. 235 (2005) 272.
[29] T. Kamegawa, R. Takeuchi, M. Matsuoka, M. Anpo, Catal. Today 111 (2006) 248.
[30] M. Anpo, J.M. Thomas, Chem. Commun. (2006) 3273.
[31] H. Yamashita, K. Yoshizawa, M. Ariyuki, S. Higashimoto, M. Che, M. Anpo, Chem. Commun. (2001) 435.
[32] T. Kamegawa, J. Morishima, M. Matsuoka, J.M. Thomas, M. Anpo, J. Phys. Chem. C 111 (2007 1076).
[33] H. Yamashita, S. Kawasaki, Y. Ichihashi, M. Harada, M. Takeuchi, M. Anpo, G. Stewart, M.A. Fox, C. Louis, M. Che, J. Phys. Chem. B 102 (1998) 5870.
[34] H. Yamashita, M. Honda, M. Harada, Y. Ichihashi, M. Anpo, T. Hirao, N. Itoh, N. Iwamoto, J. Phys. Chem. B 102 (1998) 10707.
[35] H. Yamashita, Y. Ichihashi, M. Harada, G. Stewart, M.A. Fox, M. Anpo, J. Catal. 158 (1996) 97.
[36] H. Yamashita, N. Kamada, H. He, K. Tanaka, S. Ehara, M. Anpo, Chem. Lett. (1994) 855.
[37] M. Anpo, K. Chiba, J. Mol. Catal. 74 (1992) 207.
[38] R. Nakamura, A. Okamoto, H. Osawa, H. Irie, K. Hashimoto, J. Am. Chem. Soc. 129 (2007) 9596.
[39] T. Tanaka, H. Yamashita, R. Tsuchitani, T. Funabiki, S. Yoshida, J. Chem. Soc., Faraday Trans. 1 (84) (1988) 2987.
[40] M. Matsuoka, T. Kamegawa, M. Anpo, in: G. Ertl, H. Knözinger, F. Schüth, J. Weitkamp (Eds.), Handbook of Heterogeneous Catalysis, Wiley–VCH, 2008, p. p. 1065.
[41] M. Anpo, M. Matsuoka, in: K.D.M. Harris, P. Edwards (Eds.), Turning Points in Solid-State, Materials and Surface Science, RSC Publishing, 2008, p. p. 496.
[42] F. Amano, T. Ito, S. Takenaka, T. Tanaka, J. Phys. Chem. B 109 (2005) 10973.
[43] T. Tanaka, S. Takenaka, T. Funabiki, S. Yoshida, Chem. Lett. (1994) 1585.
[44] M.J. Nash, S. Rykov, R.F. Lobo, D.J. Doren, I. Wachs, J. Phys. Chem. C 111 (2007) 7029.
[45] A.A. Lisachenko, K.S. Chikhachev, M.N. Zakharov, L.L. Basov, B.N. Shelimov, I.R. Subbotina, M. Che, S. Coluccia, Top. Catal. 20 (2002) 119.
[46] A. Siani, D.K. Captain, O.S. Alexeev, E. Stafyla, A.B. Hungria, P.A. Midgley, J.M. Thomas, R.D. Adams, M.D. Amiridis, Langmuir 22 (2006) 5160.
[47] M.F. Hazenkamp, G. Blasse, J. Phys. Chem. 96 (1992) 3442.
[48] S.Y. Chin, O.S. Alexeev, M.D. Amiridis, Appl. Catal A: Gen. 286 (2005) 157.
[49] A. Manasilp, E. Gulari, Appl. Catal. B 37 (2004) 17.
[50] T.V. Choudhary, D.W. Goodman, Catal. Today 77 (2002) 65.
[51] E. Groppo, C. Lamberti, S. Bordiga, G. Spoto, A. Zecchina, Chem. Rev. 105 (2005) 115.
[52] C. Murata, H. Yoshida, T. Hattori, Chem. Commun. (2001) 2412.
[53] N.J. Turro (Ed.), Modern Molecular Photochemistry, Benjamin/Cummings, New York, 1978.